Rapid onset of ocean anoxia shown by high U and low Mo isotope compositions of sapropel S1

M.B. Andersen, A. Matthews, M. Bar-Matthews, D. Vance

Supplementary Information

The Supplementary Information includes:

1. Methods

The samples from sapropel S1 were taken from ODP core 967D, drilled at a water depth of 2550m south of Cyprus, at the base of the northern slope of the Eratosthenes Seamount (Emeis *et al.*, 1998) (Fig. S-1). This study uses the dried and sieved <63µm fraction of the samples analysed by Scrivner *et al.* (2004) and Vance *et al.* (2004) for Nd isotope measurements in foraminifera (ODP 967D-1H1, covering S1 and depths immediately above and below). The S5 data of Andersen *et al.* (2018) used in this study were also measured on the dried and sieved <63 µm fraction of the samples analysed by Scrivner *et al.* (2004) for Nd isotopes in foraminifera (ODP 967C-H5). Previous studies using the <63 µm fractions indicate that they provide a representative record of the elemental and isotope geochemistry of sapropels (Box *et al.*, 2011; Azrieli-Tal *et al.*, 2014). Sample preparation and U isotope measurements were conducted at the facilities of the Bristol Isotope Group, University of Bristol, United Kingdom, while chemical analyses of major and trace element chemical analyses (wt.% and µg/g, respectively) were made using Induction Coupled Optical Emission Spectroscopy (ICP-OES) and Inductively Coupled Plasma Mass Spectrometry (ICP-MS) at the Geological

Survey of Israel after low temperature ashing and sodium peroxide digestions. Errors on single values (1σ) are from ±5 % and ±7 % for ratios. Total organic carbon (TOC) data (for the bulk sediment) are taken from Vance *et al.* (2004). For samples missing a direct TOC measurement, the TOC is estimated as an average of the two bracketing samples with available TOC data.
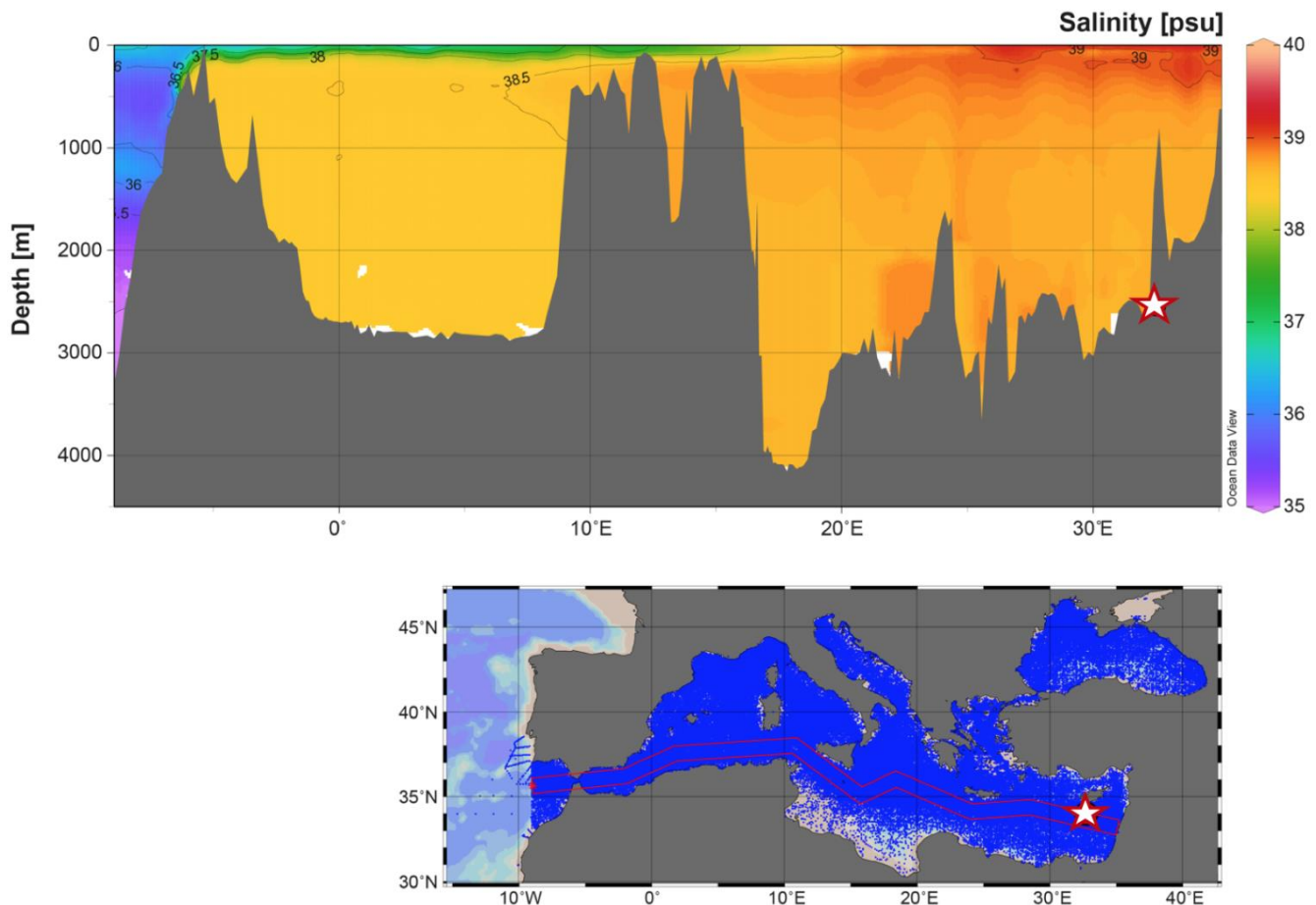

Figure S-1   Vertical salinity profile (top) through the present-day Mediterranean basin (bottom). The position of core ODP 967 (2550 m water depth) is marked (star). Present-day deep-waters are well oxygenated due to thermohaline circulation driven by surface water evaporation and high salinity in the EM. The periodic formation of organic carbon-rich sapropels correlated with high northern hemisphere summer insolation during minima in the *ca* 21 ka orbital precession cycle. Significantly slower deep-water renewal rates in the EM would have played an important role in the formation of sapropels and are consistent with the suppression of overturning during high insolation periods, due to increased water body stratification resulting from higher riverine freshwater input under enhanced monsoon forcing. Diagram generated in Ocean Data View (https://odv.awi.de).

Details of the molybdenum and uranium isotope analyses, including standards, calibration procedures, and error treatments, are given in Azrieli-Tal *et al.* (2014) and Andersen *et al.* (2018). In brief, for the uranium isotope work in this study, samples (10-50 mg) were dissolved in steps involving concentrated HNO_3, HF, HCl and H_2O_2. At the first dissolution step, in HNO_3 and HF, the IRMM3636 $^{236}U/^{233}U$ double spike was added, aiming for a $^{236}U/^{235}U$ of ~4. After heating, fluxing and subsequent drying steps using 6 M HCl (x2) and a 7 M HNO_3 + 30% H_2O_2 mixture were completed, samples were re-dissolved in 10 ml of 3 M HNO_3 in preparation for U-Teva chromatographic chemistry, following protocols given in Andersen *et al.* (2014; 2018). Purified U fractions were dried and prepared for mass spectrometry in 2% (v/v) HCl aiming for 100-200 ppb U. Full procedural chemistry blanks were <20 pg of U. Uranium isotopic analyses were carried out at the University of Bristol, using a ThermoQuest Neptune instrument operating at low mass resolution (M/ΔM

~500) by means of a CPI (Amsterdam, The Netherlands) PFA nebulizer and spray chamber fitted to a CETAC Aridus. The set-up and measurement protocols were as outlined in Andersen *et al.* (2014; 2015). All Faraday cups were equipped with $10^{11}\,\Omega$ resistors, apart from the cup for ^{238}U ($10^{10}\,\Omega$). Measurements were conducted with "standard" sampler and "X" type skimmer cones. Typical sample ion beam intensities were ~1 nA for ^{238}U using ~50 ng U per analysis. Measurements of two unknowns were bracketed with the CRM-145 uranium standard, spiked in similar fashion as the unknowns. The in-house CZ-1 uraninite standard, processed through U-Teva chemistry and periodically measured in a similar fashion to the sediment samples, yielded $\delta^{238}U$ of –0.055±0.032 (±2S.D.) for ten repeats, in excellent agreement with previously published compositions for this standard (Stirling *et al.*, 2007; Andersen *et al.*, 2015). The $^{234}U/^{238}U$ ratios were measured simultaneously with the $^{235}U/^{238}U$, and the $^{234}U/^{238}U$ data are reported as $\delta^{234}U$, the $^{234}U/^{238}U$ relative to secular equilibrium in part per thousand using the half-lives of Cheng *et al.* (2013). The external reproducibility for the CZ-1 standard is used as the uncertainty estimate for each of the unknowns (Andersen *et al.*, 2014; 2015; 2018). Sample data, including depth information, chemical element concentrations, and isotopic compositions used in this study are presented in Table S-1.

2. Age Model and Sapropel Event Definitions

The age model for S1 (10.8 to 6.1 ka) is taken from de Lange *et al.* (2008) and from Grant *et al.* (2012) for S5 (128.3 to 121.5 ka). The upper and lower boundaries assigned to the sapropels S1 and S5 are determined from their Ba/Al and TOC profiles (130-106 cm and 103.5- 74 cm, respectively; Azrieli-Tal *et al.*, 2014; Andersen *et al.*, 2018, see Figure S-2). Whereas the TOC and Ba/Al boundaries coincide in S5, the TOC profile in S1 indicates post-sapropel oxidation (burndown) in its upper 4 cm (106-110 cm) (Fig. S-2). Sapropel geochemical data for S1 *sensu stricto* are thus recorded from ~110 to 130 cm. Furthermore, a short-lived oxidation event commencing at ~116 cm is also evident from the molybdenum isotope, Fe/Al and Ba/Al data (Azrieli- Tal *et al.*, 2014). This likely correlates with a re-ventilation event related to the 8 ka northern hemisphere cold climate event recorded in other EM S1 sapropels (Casford *et al.*, 2003). This injection of oxygen by re-ventilation has been recognised in number of sapropel S1 samples and is shown to affect (in addition to Ba/Al) redox sensitive metal ratios such as Fe/Al, As/Al and V/Al (Hennekam *et al.*, 2014 ; Tachikawa *et al.*, 2015 ; Filippidi and de Lange, 2019). The preservation in ODP967 of this re-ventilation signal (which has lead researchers to classify S1 into early (S1a) and late (S1b) segments) is not consistent with post-sapropel diagenetic remobilization of reduction sensitive metals from upper S1b into lower S1a. Specifically for U, a re-distribution profile would be expected to show increasing U/Al from the top and down to a zone of maximum reduction within S1a, similar to observed in modern reducing sediments with increasing uptake of reduced U at depth (*e.g.,* Abshire *et al.*, 2020). The lack of such U (Fig. 1) or U/Al (Fig. S-2) profile, combined with the TOC and Ba/Al profiles for S1 and S5, is compatible with the early/late peak sapropel development evident in redox sensitive elements (Fig. S-2). This is also true for EM S1 and S5 TOC, Ba/Al and redox metal sapropel profiles determined in other studies (*e.g.,* Gallego-Torres *et al.*, 2007; 2010).
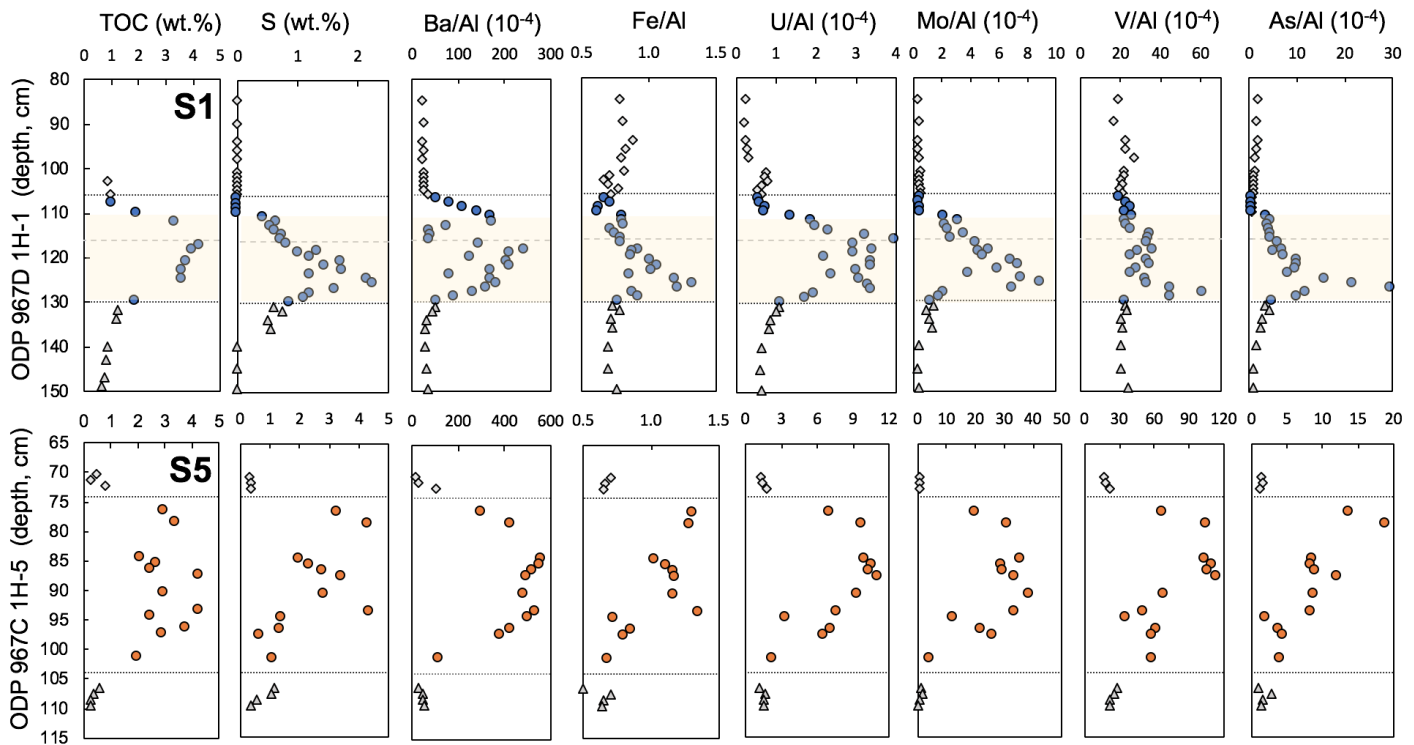
Figure S-2   Depth profiles of selected proxies (TOC, S, Ba/Al, Fe/Al, U/Al, Mo/Al, V/Al, As/Al) for sapropel S1 (top layer) and sapropel S5 (lower layer). (Data sources for this figure and main text Figure 1, S1: Azrieli-Tal *et al.*, 2014; Vance *et al.*, 2004; this study; S5: Andersen *et al.*, 2018; Emeis *et al.*, 1998 –see Table S-1). Stippled lines represent sapropel boundaries. The additional dashed line at 116 cm in S1 represents the commencement of the 8 ka reventilation event, and the yellow shading defines the unaltered sapropel below the depth to which the effects of the post-sapropel burndown were felt. The data clearly show the different timing of the peak increase in redox sensitive proxies early in S1 *vs*. late in S5. Note the different scales between S1 and S5 for a range of elemental and ratios (S, Ba/Al, U/Al, Mo/Al, V/Al, As/Al).

3. *Organic Carbon Sediment Accumulation Rates*

Organic carbon accumulation rates (OCAR) at peak sapropel conditions were calculated using the equation OCAR = 1000 * TOC * ρ * LSR mg/cm^2.ky (Gallego-Torres *et al.*, 2007; Algeo *et al.*, 2013; Schoepfer *et al.*, 2015), where ρ is the dry sediment density and TOC is the mean TOC wt. fraction (g/g). Mean TOC fraction (Fig. S-2) and standard deviation (1SD) data are 0.0382 ± 0.0028 for peak S1 data (126-118 cm) and 0.0316 ± 0.0.77 for peak S5 data (94-76 cm). S1 and S5 have similar thicknesses at ODP 967 (24 vs 29.5 cm), but the longer duration of S5 (6.8 *vs*. 4.7 ky) means that it has a slightly lower linear sedimentation rate (LSR) of 4.3 cm/ky compared to 5.1 cm/ky for S1). The ρ values are taken from S1 and S5 data at EM ODP site 964 (1.34 ±0.08 and 1.31 ± 0.03 g/cm^3, respectively (Gallego-Torres *et al.*, 2007)). Calculated OCAR values at ODP 967 are: 261 ± 36 mg/cm^2.ky (S1): 178 ± 48 mg/cm^2.ky (S5). These values are comparable with average OCAR values calculated for the Black Sea (Schoepfer *et al.*, 2015) and emphasise the fact that peak S1 has a high organic carbon flux, despite apparently lower deep-water sulfide levels than S5.

4. Authigenic U and Mo Concentration and Isotope Estimates

Authigenic U (U_{auth}) and molybdenum (Mo_{auth}) were calculated from the U and Mo enrichment factors relative to Post Archaean Average Shale (PAAS; Taylor & McLennan, 1985) U/Al and Mo/Al ratios, which are taken to represent the detrital component (Thomson *et al*., 1999; Brumsack, 2006; Tribovillard *et al*., 2006). Such a calculation (Table S-1) shows that the detrital fraction (U_{det}) is a significant component of the background sediments: overlying post-sapropel sediments U_{det} ~ 50% falling to < 20% within 5 cm of the boundary: Mo_{det} ~ 50% falling to ~ 30%; underlying pre-sapropel sediments U_{det} ~ 19-11%; Mo_{det} ~ 46-15%. U_{auth} and Mo_{auth} fractions in S1 vary from 85% to 99%, with values >96% typical of peak sapropel conditions.

These detrital U estimates are consistent with the measured $\delta^{234}U$ (Table S-1). The Holocene age of the samples means that the age correction for the $\delta^{234}U$ is less than a few permil and the sapropels are likely to have experienced minimal ^{234}U nuclide redistribution, as has been observed in other sapropels (Gourgiotis *et al*., 2011), and is also likely the case for the S5 samples (Table S-1). The $\delta^{234}U$ values are high for S1 (~130-115‰), slightly lower for pre-S1 (~110-100‰) and lowest for post-S1 (~90-0‰) sediments. While modern seawater has a $\delta^{234}U$ of ~146‰, the detrital material can be variable and deviate from secular equilibrium. It is therefore not possible to accurately estimate the authigenic U fraction in the absence of good estimates of the detrital terrigenous $\delta^{234}U$ composition. We note however that the $\delta^{234}U$ compositions from highest to lowest values of S1, followed by pre-S1 and then post-S1, are in good agreement with the order of high to low authigenic U based on U/Al.

The isotope composition of the authigenic Mo and U fractions is estimated using the elemental concentrations in combination with Mo and U isotope compositions for detrital terrigenous shales. Here, values of $\delta^{238}U$ = -0.3‰ and $\delta^{98}Mo$ = 0‰ were used for the detrital terrigenous sediments (Tissot & Dauphas, 2015; Andersen *et al*., 2017; Kendall *et al*., 2017; Andersen *et al*., 2018). Propagation of uncertainties on the authigenic composition was done by weighting the relative size of the detrital component following Andersen *et al*., (2014) and (2018), see Table S-1. Furthermore, authigenic $\delta^{238}U$ and $\delta^{98}Mo$ from literature data (Asael *et al*., 2013 ; Kendall *et al*., 2015; Cheng *et al*., 2020; Kendall *et al*., 2020) was reconverted in similar fashion to the sapropel data (apart from omitting the 'carbonate' correction for the authigenic U, see below) and using Mo-U isotope and Mo-U *vs*. Al ratios reported in these publications (Table S-1).

5. Authigenic $\delta^{238}U$ and $\delta^{98}Mo$ - Estimating the Contribution from U and Mo Directly Associated with Organic Matter

Andersen *et al*. (2014) suggested that authigenic U was dominated by two main fractions, (i) U from biogenic carbonates and (ii) U incorporated from *in situ* uranium reduction. Following calculations in Andersen *et al*. (2014), which assume that the [Ca] in bulk sediments is primarily from biogenic carbonates with ~1 ppm U, the relative U contribution from this carbonate source to the authigenic fraction can be estimated. This calculation shows that the biogenic carbonate U fraction constitutes <3% for S1 and <20% for surrounding sediments (Table S-1). Further, the $\delta^{238}U$ of the remaining authigenic U fraction may be estimated by subtracting the biogenic U carbonate fraction with $\delta^{238}U$ = -0.4‰ (Andersen *et al.*, 2014). These calculations suggest that the greater part of U_{auth} in these sediments is due to authigenic U addition rather than that associated with biogenic carbonates. In addition to U uptake from *in situ* U reduction (process ii), it has also been suggested that U may be directly associated with organic matter (OM) which could be a third (iii) potential important additional source of authigenic U accumulation in sediments. This OM-derived U, either directly incorporated or adsorbed, could carry isotopically light U to the sediments (Holmden *et al.*, 2015; Hinojosa *et al.*, 2016; Andersen *et al.*, 2017; Abshire *et al.*, 2020; Chen *et al.*, 2020). Such a U fraction would

be indistinguishable from the *in situ* uranium reduction component (process ii) in the calculations described above, and may drive the authigenic $\delta^{238}U$ pool towards lower compositions, in instances when the relative OM deposition rate *vs*. *in situ* reduction rate is high.

Focusing on the pre-S1 and early part of the S1 data with relatively low [U_{auth}] in the sediments, 1/[U_{auth}] *vs*. $\delta^{238}U$ plots (Fig S-3a) show a systematic evolution from low $\delta^{238}U_{auth}$ (~ -0.6‰) at low [U_{auth}], to high $\delta^{238}U_{auth}$ (~ +0.5‰) at high [U_{auth}]. This pattern is consistent with an approximate mixing trend between authigenic OM-derived U ($\delta^{238}U$ ~ -0.6) and increasingly *in situ* U reduction. The 1/[U_{auth}] *vs*. $\delta^{238}U$ plots for the S1 and S5 and background sediment data (Fig S-3b) show that the post-S1 data also plot in the region that may be dominated by authigenic OM-derived U, but with significantly lower [U_{auth}]. Also, both the post- and pre-S5 data show moderate U enrichments, which could suggest a mixture between authigenic OM-derived U and *in situ* U reduction. On the other hand, Andersen *et al*. (2018) interpreted these samples to show U and Mo isotope systematics consistent with near quantitative uptake of U and Mo from porewaters. Both scenarios are possible. In contrast, both peak S1 and peak S5 appear to be completely dominated by authigenic *in situ* U reduction uptake, but with differently expressed U isotope fractionations as discussed in the main text.
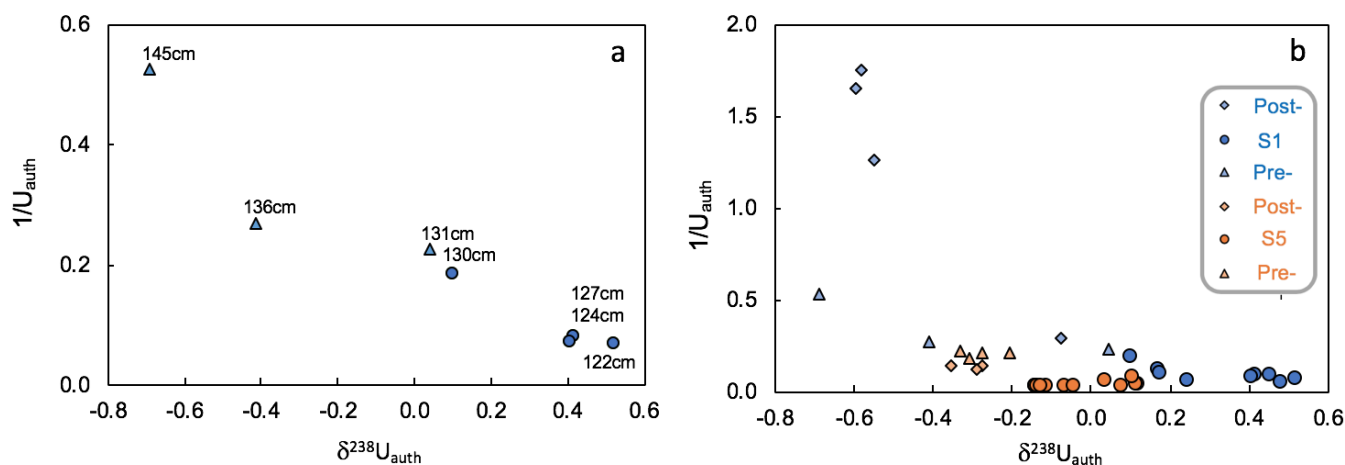

Figure S-3 **(a)** Cross-plots of $\delta^{238}U$ vs. 1/U_{auth} (ppm^{-1}) from pre-S1 and the early part of S1 (from 145 to 120 cm depth) and **(b)** all the data from S1/S5 and surrounding sediments. The $\delta^{238}U$ vs. 1/U_{auth} plot in (a) suggests that the data define a possible mixing trend between authigenic U associated with organic matter ($\delta^{238}U$ ~ -0.6‰ and low U_{auth}) and U formed by in situ reduction ($\delta^{238}U$ ~ +0.5‰ and high U_{auth}) at peak sapropel conditions.

Similar to the above discussion of the authigenic U uptake, although Mo associated with biogenic carbonate is low and therefore not important for authigenic calculations, the potential for OM-derived Mo has been suggested as a potential important source for Mo addition to organic carbon-rich sediments (e.g. McManus *et al*., 2002; King *et al*., 2018). Based on cross-plots of $\delta^{98}Mo$ *vs*. 1/[Mo_{auth}] for the S1 and S5 and surrounding data (Fig. S-4) there are no trends evident in the data which could suggest that this is an important process for the observed $\delta^{98}Mo_{auth}$ in the organic carbon-rich sapropel sediments. There is, however, a difference in the $\delta^{98}Mo_{auth}$ compositions of the background sediments. The background sediments surrounding S1 have $\delta^{98}Mo_{auth}$ values in the range of suboxic sediments with low sulfide levels, where Mo uptake could be dominated by OM or adsorption on Fe oxides (*e.g.,* McManus *et al*., 2002; Goldberg *et al*., 2009; Scholz *et al*., 2013; Matthews *et al*., 2017). On the other hand, S5 background sediments have $\delta^{98}Mo_{auth}$ values >+1.5‰, typical of sediments where authigenic Mo uptake occurs within sulfidic pore waters (Poulson-Brucker *et al*., 2009; 2012).
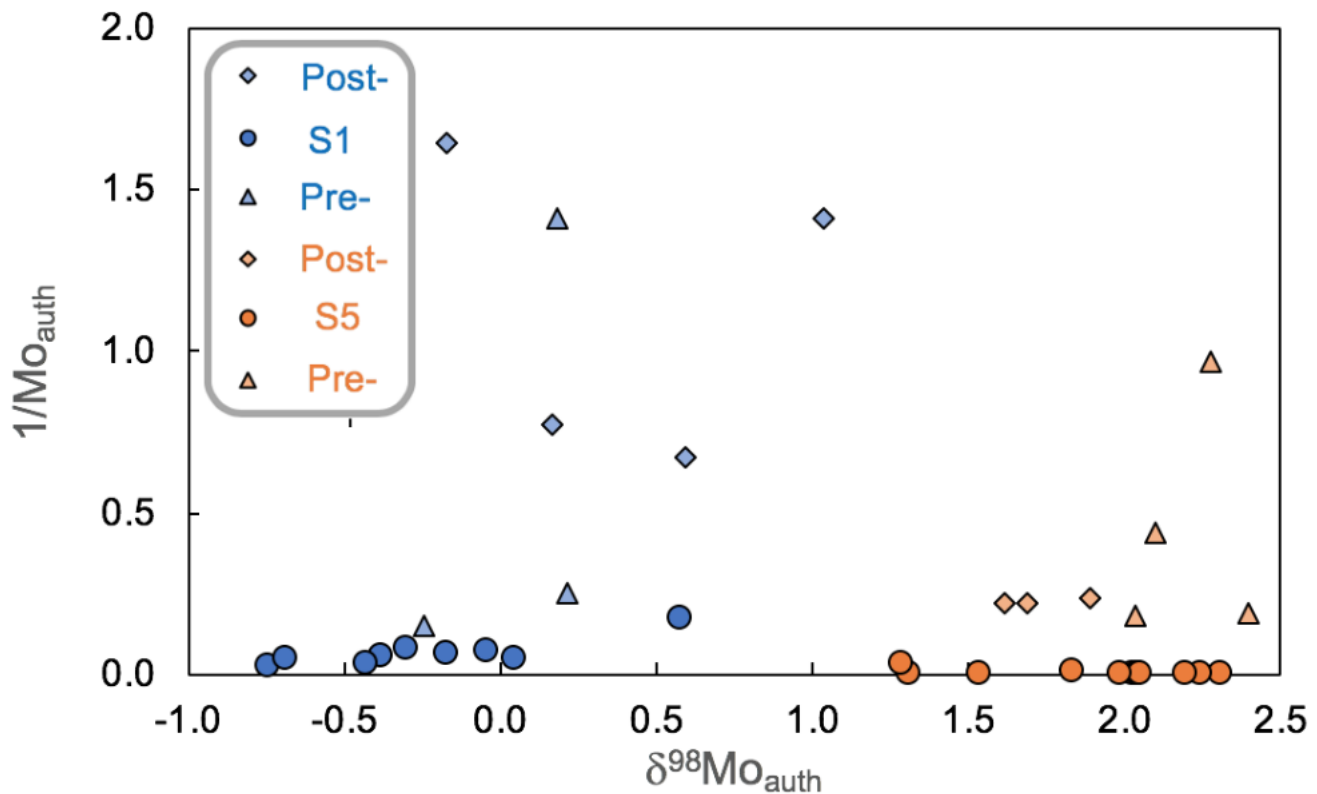
Figure S-4 δ^{98}Mo vs. 1/Mo$_{auth}$ (ppm^{-1}) cross-plot for S1 and S5 and non-sapropel sediment data. No clear mixing trends are observed between post/pre-S1 or S5 and the peak S1 and S5 sediments.

Supplementary Tables

Table S-1 is available for download (Excel file) at http://www.geochemicalperspectivesletters.org/article2027.

Table S-1   **(a)** Sapropel S1 and S5, U and Mo isotope data and concentration data, incl. authigenic estimates. **(b)** Extended trace metal concentration data for sapropel S1. **(c)** Authigenic U and Mo isotope calculations for literature data.

Supplementary Information References

Abshire, M.L., Romaniello, S.J., Kuzminov, A.M., Cofrancesco, J., Severmann, S., Riedinger, N. (2020) Uranium isotopes as a proxy for primary depositional redox conditions in organic-rich marine systems. *Earth and Planetary Science Letters* 529, 115878.

Algeo, T.J., Henderson, C.M., Tong, J., Feng, Q., Yin, H., Tyson, R.V. (2013) Plankton and productivity during the Permian–Triassic boundary crisis: An analysis of organic carbon fluxes. *Global and Planetary Change* 105, 52-67.

Andersen, M.B. Romaniello, S., Vance, D., Little, S.H., Herdman, R., Lyons, T.W. (2014) A modern framework for the interpretation of 238U/235U in studies of ancient ocean redox. *Earth and Planetary Science Letters* 400, 184-194.

Andersen, M.B., Elliott, T., Freymuth, H., Sims, K.W., Niu, Y., Kelley, K.A. (2015) The terrestrial uranium isotope cycle. *Nature* 517, 356-359.

Andersen, M.B., Stirling, C.H., Weyer, S. (2017) Uranium isotope fractionation. *Reviews in Mineralogy and Geochemistry* 82, 799-850.

Andersen, M.B., Matthews, A., Vance, D., Bar-Matthews, M., Archer, C., de Souza, G.F. (2018) A 10-fold decline in the deep Eastern Mediterranean thermohaline overturning circulation during the last interglacial period. *Earth and Planetary Science Letters* 503, 58-67.

Asael D, Tissot FL, Reinhard CT, Rouxel O, Dauphas N, Lyons TW, Ponzevera E, Liorzou C, Chéron S. (2013) Coupled molybdenum, iron and uranium stable isotopes as oceanic paleoredox proxies during the Paleoproterozoic Shunga Event. *Chemical Geology* 362,193–210.

Azrieli-Tal, I., Matthews, A., Bar-Matthews, M., Almogi-Labin, A., Vance, D., Archer, C., Teutsch, N. (2014) Evidence from molybdenum and iron isotopes and molybdenum–uranium covariation for sulphidic bottom waters during Eastern Mediterranean sapropel S1 formation. *Earth and Planetary Science Letters* 393, 231-242.

Box, M.R., Krom, M.D., Cliff, R.A., Bar-Matthews, M., Almogi-Labin, A., Ayalon, A., Paterne, M. (2011) Response of the Nile and its catchment to millennial-scale climatic change since the LGM from Sr isotopes and major elements of East Mediterranean sediments. *Quaternary Science Reviews* 30, 431-442.

Brumsack, H.-J. (2006) The trace metal content of recent organic carbon-rich sediments: Implications for Cretaceous black shale formation, *Palaeogeography, Palaeoclimatology, Palaeoecol*ogy, 232, 344-361.

Casford, J. S. L., Rohling, E. J., Abu-Zied, R. H., Fontanier, C., Jorissen, F. J., Leng, M. J., Schmiedl, G., Thomson, J. (2003) A dynamic concept for eastern Mediterranean circulation and oxygenation during sapropel formation. *Palaeogeography, Palaeoclimatology, Palaeoecology* 190, 103–119.

Chen, X., Zheng, W., Anbar, A.D. (2020) Uranium Isotope Fractionation (238U/235U) during U (VI) Uptake by Freshwater Plankton. *Environmental Science & Technology* 54, 2744-2752.

Cheng, H., Edwards, R.L., Sehe, C.C ., Polyak, V.J., Asmerom, Y., Woodhead, Y., Hellstrom, J., Wang, Y., Kong, X., Spötl, C., Wang, X. and Alexander Jr., C. (2013) Improvements in ^{230}Th dating, ^{230}Th and ^{234}U half-life values, and U-Th isotopic measurements by multi-collector inductively couples plasma mass spectrometry. *Earth and Planetary Science Letters* 371-372, 82-91.

Cheng, M., Li, C., Jin, C., Wang, H., Algeo, T.J., Lyons, T.W., Zhang, F. and Anbar, A. (2020) Evidence for high organic carbon export to the early Cambrian seafloor. *Geochimica et Cosmochimica Acta, doi:* 10.1016/j.gca.2020.01.050.

de Lange, G.J., Thomson, J., Reitz, A., Slomp, C.P., Speranza Principato, M., Erba, E., Corselli, C. (2008) Synchronous basin-wide formation and redox-controlled preservation of a Mediterranean sapropel. *Nature Geoscience* 1, 606–610.

Emeis, K.C., Schulz, H.M., Struck, U., Sakamoto, T., Doose, H., Erlenkeuser, H., Howell, M., Kroon, D., Paterne, M. (1998) Stable isotope and alkenone temperature records of sapropels from sites 964 and 967: constraining the physical environment of sapropel formation in the eastern Mediterranean sea. In: Robertson, A.H.F., Emeis, K.C., Richter, C., Camerlenghi, A. (Eds.) *Proceedings of the Ocean Drilling Program, Scientific Results* 160, 309-331.

Filippidi, A. & de Lange G.J. (2019) Eastern Mediterranean deep water formation during sapropel S1: a reconstruction using geochemical records along a bathymetric transect in the Adriatic outflow region. *Paleoceanography and Paleoclimatology*, 34, 409–429. doi: 10.1029/2018PA003459.

Gallego-Torres, D., Martínez-Ruiz, F., Paytan, A., Jiménez-Espejo, F.J., Ortega-Huertas, M. (2007) Pliocene–Holocene evolution of depositional conditions in the eastern Mediterranean: role of anoxia vs. productivity at time of sapropel deposition. *Palaeogeography, Palaeoclimatology, Palaeoecology* 246, 424–439.

Gallego-Torres, D., Martinez-Ruiz, F., de Lange, G. J., Jimenez-Espejo, F.J. Ortega-Huertas, M. (2010) Trace-elemental derived paleoceanographic and paleoclimatic conditions for Pleistocene Eastern Mediterranean sapropels. *Palaeogeography, Palaeoclimatology, Palaeoecology* 293, 76–89.

Goldberg, T., Archer, C., Vance, D., Poulton, S.W. (2009) Mo isotope fractionation during adsorption to Fe (oxyhydr)oxides. *Geochimica Cosmochimica Acta* 73, 6502–6516.

Gourgiotis A., Reyss, J.L., Frank, N., Guihou, A., Anagnostou, C. (2011) Uranium and radium diffusion in organic-rich sediments (sapropels). *Geochemistry, Geophysics, Geosystems* 12, Q09012.

Grant, K.M., Rohling, E.J., Bar-Matthews, M., Ayalon, A., Medina-Elizalde, M., Ramsey, C.B., Satow, C., Roberts, A.P. (2012) Rapid coupling between ice volume and polar temperature over the past 150,000 years. *Nature* 491, 744-747.

Hennekam, R., Jilbert, T., Schnetger, B., de Lange, G.J. (2014) Solar forcing of Nile discharge and sapropel S1 formation in the early to middle Holocene eastern Mediterranean. *Paleoceanography* 29, 2013PA002553, doi:10.1002/2013PA002553.

Hinojosa, J.L., Stirling, C.H., Reid, M.R., Moy, C.M., Wilson, G.S. (2016) Trace metal cycling and $^{238}U/^{235}U$ in New Zealand's fjords: Implications for reconstructing global paleoredox conditions in organic-rich sediments. *Geochimica et Cosmochimica Acta* 179, 89-109.

Holmden, C., Amini, M., Francois, R. (2015) Uranium isotope fractionation in Saanich Inlet: A modern analog study of a paleoredox tracer. *Geochimica et Cosmochimica Acta* 153, 202-215.

Kendall, B., Komiya, T., Lyons, T.W., Bates, S.M., Gordon, G.W., Romaniello, S.J., Jiang, G., Creaser, R.A., Xiao, S., McFadden, K., Sawaki, Y. (2015) Uranium and molybdenum isotope evidence for an episode of widespread ocean oxygenation during the late Ediacaran Period. *Geochimica et Cosmochimica Acta* 156, 173-193.

Kendall, B., Dahl, T.W., Anbar, A.D. (2017) The stable isotope geochemistry of molybdenum. *Reviews in Mineralogy and Geochemistry* 82, 683-732.

Kendall, B., Wang, J., Zheng, W., Romaniello, S.J., Over, D.J., Bennett, Y., Xing, L., Kunert, A., Boyes, C., Liu, J. (2020) Inverse correlation between the molybdenum and uranium isotope compositions of Upper Devonian black shales caused by changes in local depositional conditions rather than global ocean redox variations. *Geochimica et Cosmochimica Acta*, doi: 10.1016/j.gca.2020.01.026

King, E.K., Perakis, S.S., Pett-Ridge, J.C. (2018) Molybdenum isotope fractionation during adsorption to organic matter. *Geochimica et Cosmochim. Acta* 222, 584-598.

Matthews, A., Azrieli-Tal, I., Benkovitz, A., Bar-Matthews, M., Vance, D., Poulton, S.W., Teutsch, N., Almogi-Labin, A., Archer, C. (2017) Anoxic development of sapropel S1 in the Nile Fan inferred from redox sensitive proxies, Fe speciation, Fe and Mo isotopes. *Chemical Geology* 475, 24-39.

McManus, J., Nägler, T.F., Siebert, C., Wheat, C.G., Hammond, D.E. (2002) Oceanic molybdenum isotope fractionation: Diagenesis and hydrothermal ridge-flank alteration. *Geochemistry, Geophysics, Geosystems* 3, 1-9.

Poulson-Brucker, R.L., McManus, J., Severmann, S., Berelson, W.M. (2009) Molybdenum behavior during early diagenesis: insights from Mo isotopes. *Geochemistry, Geophysics, Geosystems* 10, doi: 10.1029/2008GC002180.

Poulson-Brucker, R.L., McManus, J., Poulton, S.W. (2012) Molybdenum isotope fractionation observed under anoxic experimental conditions. *Geochemical Journal* 46, 201-209.

Schoepfer, S.D., Shen, J., Wei, H., Tyson, R.V., Ingall, E., Algeo, T.J. (2015) Total organic carbon, organic phosphorus, and biogenic barium fluxes as proxies for paleomarine productivity. *Earth-Sciences Reviews* 149, 23-52.

Scholz, F., McManus, J., Sommer, S. (2013) The manganese and iron shuttle in a modern euxinic basin and implications for molybdenum cycling at euxinic ocean margins. *Chemical Geology* 355, 56–68

Scrivner, A., Vance, D., Rohling, E.J. (2004) New neodymium isotope data quantify Nile involvement in Mediterranean anoxic episodes. *Geology* 32, 565–568.

Stirling, C.H., Andersen, M.B., Potter, E.K., Halliday, A.N. (2007) Low temperature isotopic fractionation of uranium. *Earth and Planetary Science Letters* 264, 208-225.

Tachikawa, K., Vidal, L.-A., Cornuault, M., Garcia, M., Pothin, A., Sonzogni, C., Bard, E., Menot, G., Revel, M. (2015) Eastern Mediterranean Sea circulation inferred from the conditions of S1 sapropel deposition. *Climate of the Past* 11, 855–867.

Taylor R.N., McLennan, S. (1985) *The Continental Crust: Its Composition and Evolution.* Blackwell, Boston.

Thomson, J., Mercone, D., de Lange, G.J., van Santvoort, P.J.M. (1999) Review of recent advances in the interpretation of Eastern Mediterranean sapropel S1 from geochemical evidence. *Marine Geology* 153, 77–89.

Tissot, F.L.H., Dauphas, N. (2015) Uranium isotopic compositions of the crust and ocean: age corrections, U budget and global extent of modern anoxia. *Geochimica et Cosmochimica Acta* 167,113-143.

Tribovillard, N., Algeo, T.J., Lyons, T., Riboulleau, A. (2006) Trace metals as paleoredox and paleoproductivity proxies: An update. *Chemical Geology* 232, 12-32.

Vance, D., Scrivner, A.E., Beney, P, Staubwasser, M, Henderson, G.F., Stowell, N.C. (2004) The use of foraminifera as a record of past neodymium isotope composition of seawater. *Paleoceanography* 19, PA2009. doi:10.1029/2003PA000957